Electronic Supplementary Information

Flexible temperature sensors made of aligned electrospun carbon nanofiber films with outstanding sensitivity and selectivity towards temperature

Jeng-hun Lee,[a] Haomin Chen,[a, b] Eunyoung Kim,[a] Heng Zhang,[a] Ke Wu,[a] Hongming Zhang,[a] Xi Shen,[a] Qingbin Zheng,[c] Jinglei Yang[a] and Jang-Kyo Kim[a]**

[a] Department of Mechanical and Aerospace Engineering, The Hong Kong University of Science and Technology, Clear Water Bay, Kowloon, Hong Kong
E-mail: maeshen@ust.hk (X. Shen); mejkkim@ust.hk (J. K. Kim)

[b] Prof. S. Jeon
Department of Materials Science and Engineering, Graphene Research Center of KI for the NanoCentury, Korea Advanced Institute of Science and Technology, Daejeon 305–338, Republic of Korea

[c] Prof Q. B. Zheng
School of Science and Engineering, The Chinese University of Hong Kong, Shenzhen, Guangdong 518172, China

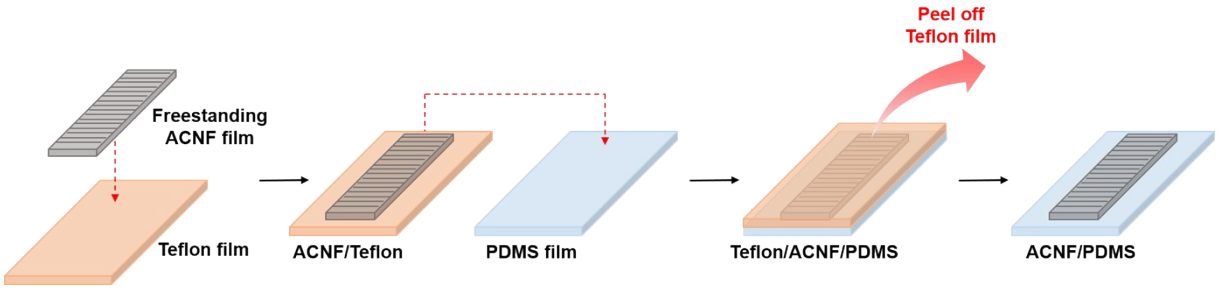

Figure S1. Schematics showing the stamp transfer of freestanding ACNF film onto PDMS substrate.

Stamp transfer of freestanding ACNF film onto the PDMS film. First, the freestanding ACNF film was placed on a Teflon film and a few drops of ethanol were applied onto the ACNF film. Upon evaporation of ethanol, the surface tension facilitated strong adhesion between the ACNF and Teflon films. Then, the Teflon film was placed on top of the PDMS film with the ACNF side facing downward and pressed with a heavy weight for 10 s. Finally, the Teflon film was gently peeled off from the PDMS film so that the ACNF film was successfully stamp transferred onto the PDMS film. Several drops of ethanol were then added onto the ACNF film to improve the adhesion between the ACNF and PDMS films.

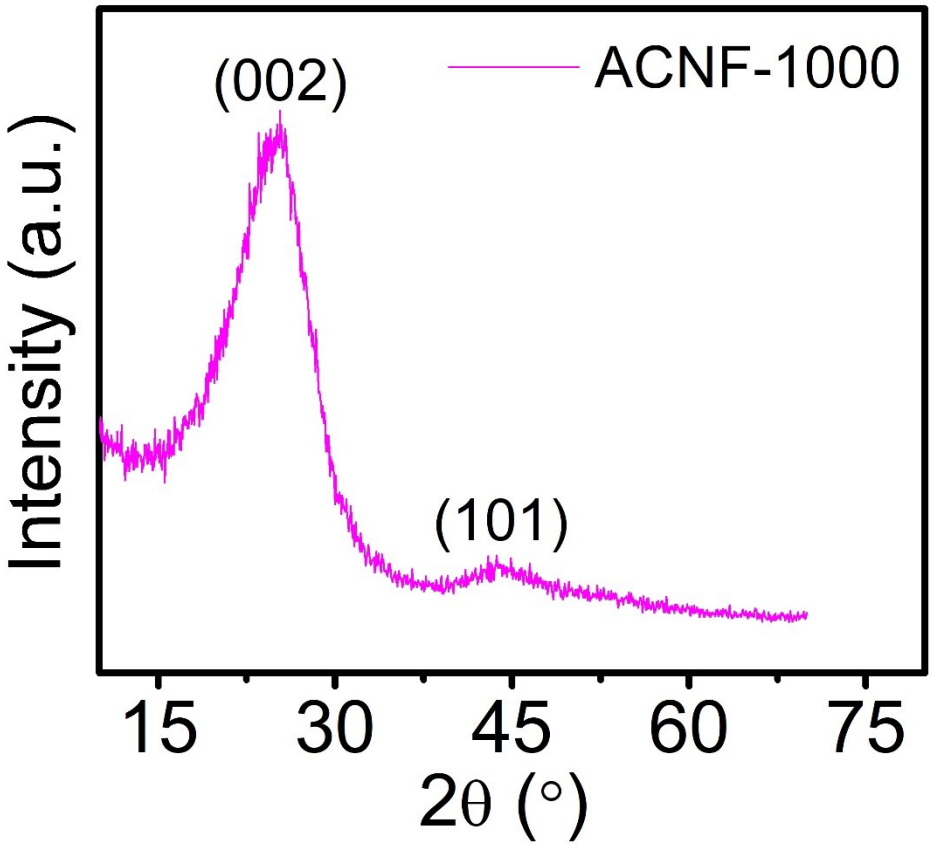

Figure S2. XRD pattern of ACNFs carbonized at 1000 ℃.

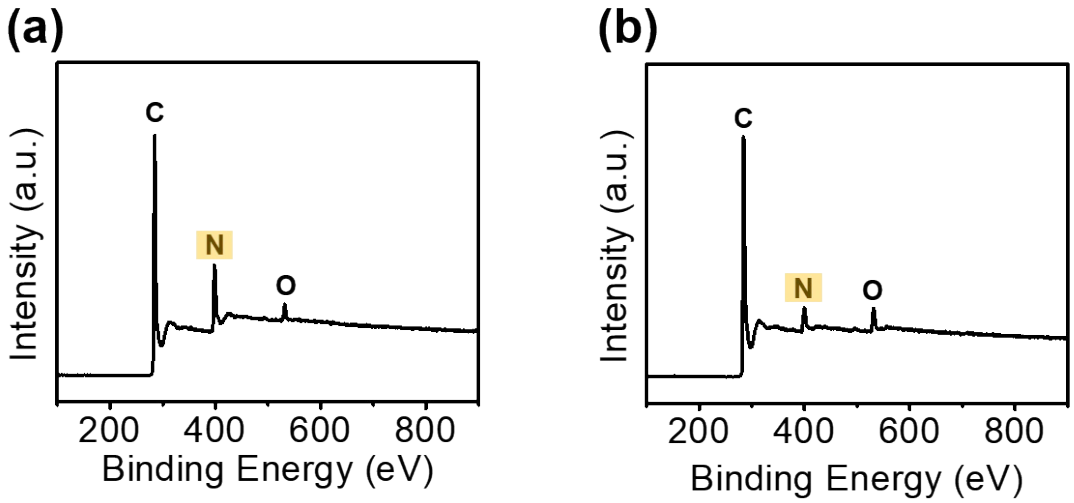

Figure S3. XPS survey spectra of ACNFs carbonized at (a) 650 ℃ and (b) 1000 ℃.

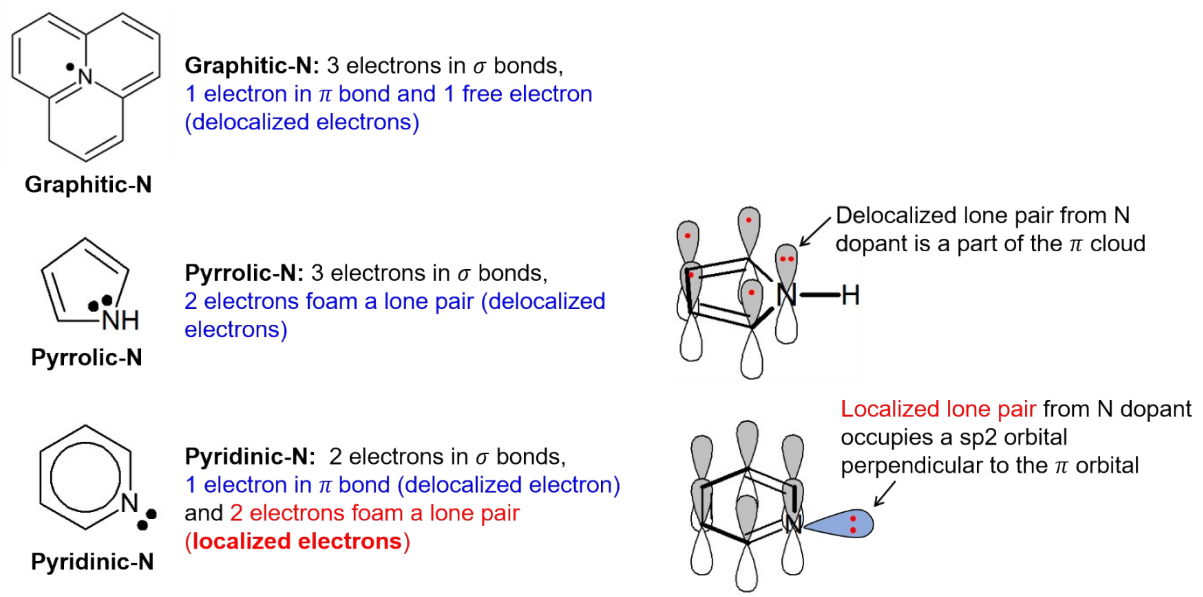

Figure S4. Electron configurations of graphitic-N, pyrrolic-N and pyridinic-N in ACNFs.

Electron configurations of graphitic-N and pyrrolic-N in ACNFs. Graphitic-N has three electrons that form σ bonds with its neighboring C atoms and two delocalized electrons, one in the π bond and the other in the π^* donor state. Pyrrolic-N also has three electrons in the σ bonds and two delocalized electrons, a lone pair existing in π cloud around the five-fold aromatic ring.

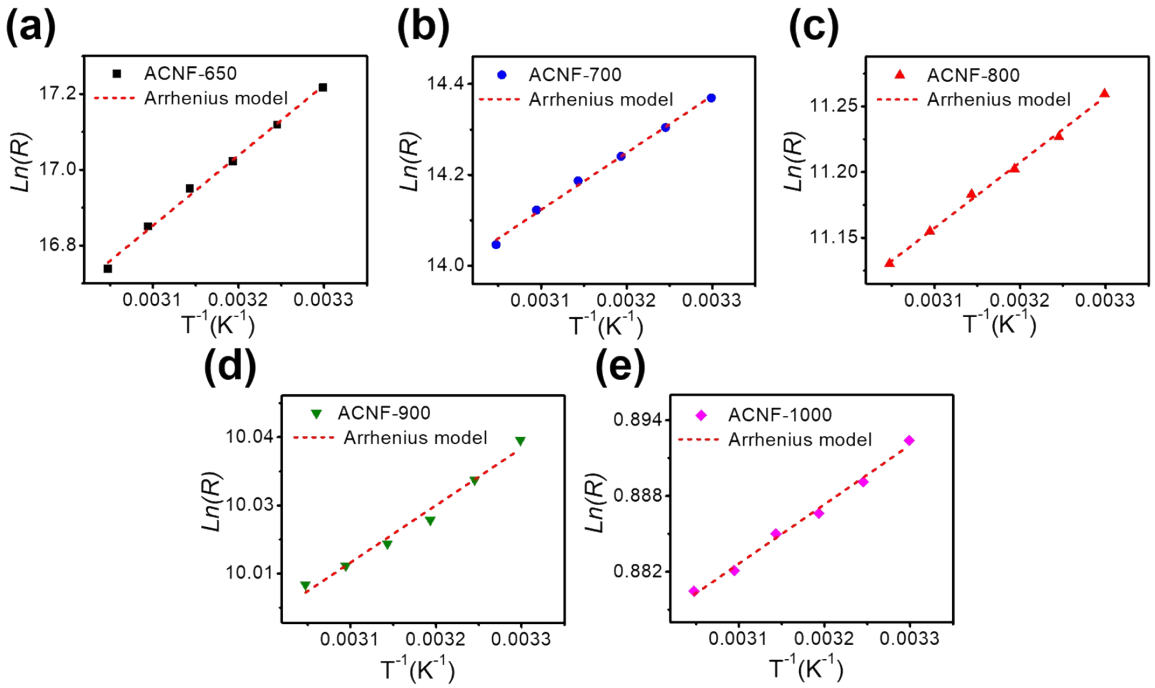

Figure S5. Plots of *ln* (R) vs T^{-1} for the ACNF temperature sensors fabricated using the ACNF films carbonized at (a) 650, (b) 700, (c) 800, (d) 900 and (e) 1000 ℃ and fitting lines using the Arrhenius model.

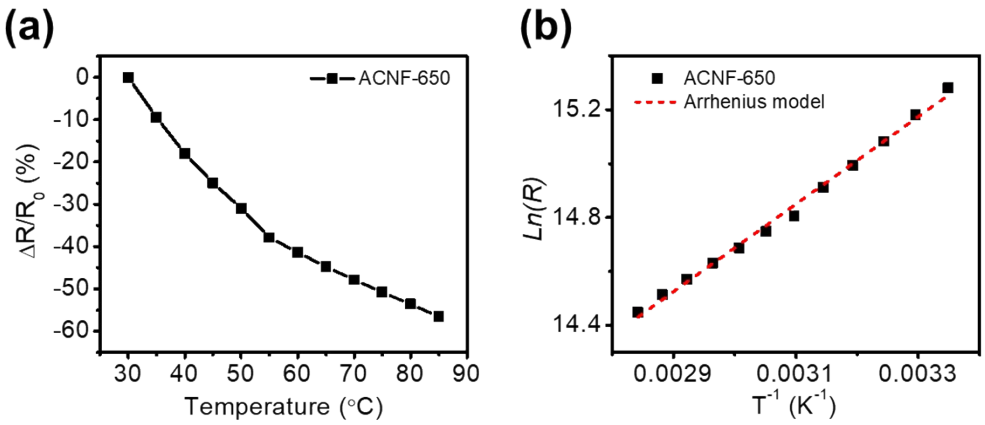

Figure S6. (a) Temperature-dependent relative resistant changes ($\Delta R/R_0$) in the temperature range from 30 to 85 °C and (b) plot of *ln* (R) vs T^{-1} for the ACNF-650 temperature sensor.

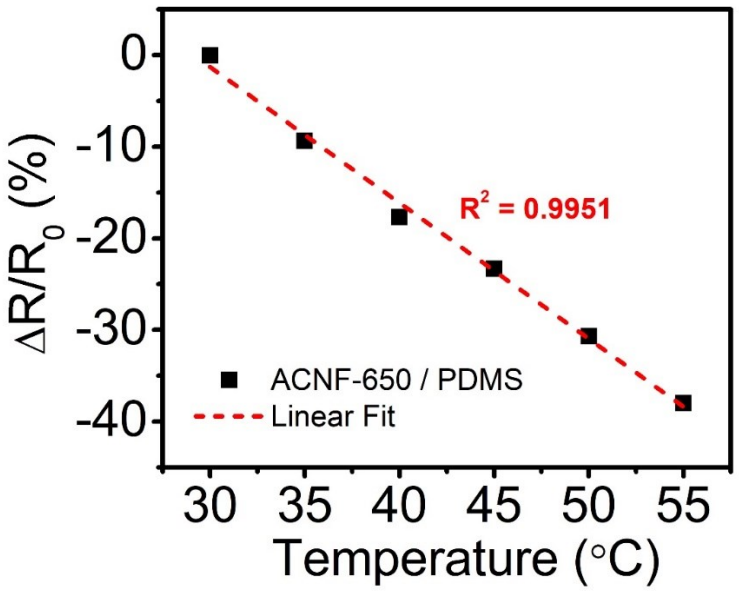

Figure S7. Linearity of the temperature sensor made using the ACNF-650 film.

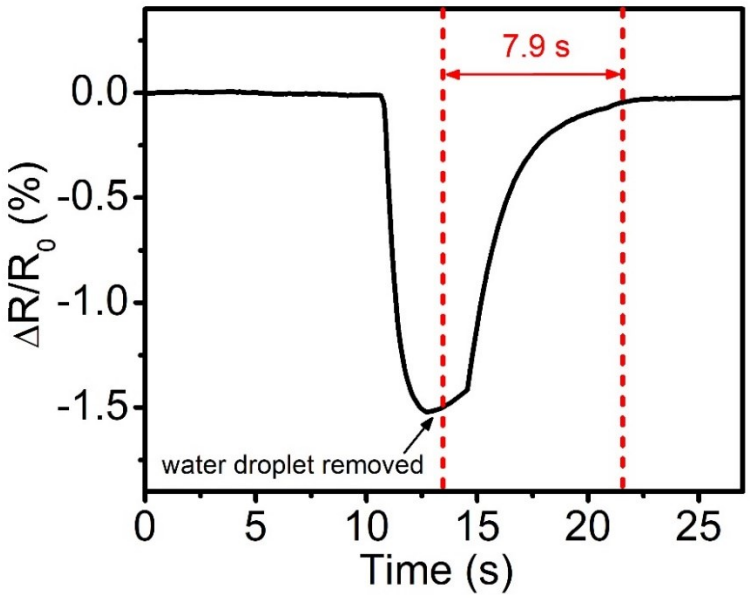

Figure S8. Recovery time of the ACNF-650 temperature sensor measured after removing a water droplet from the sensor surface with a temperature variation of around 1 ℃.

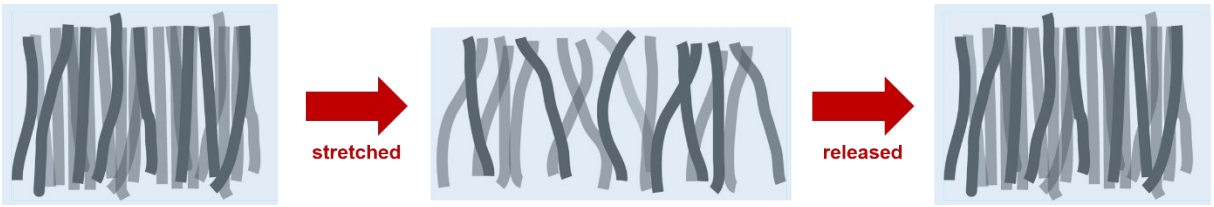

Figure S9. Schematic illustration showing the undamaged ACNF networks encapsulated by highly flexible PDMS when loaded transverse to fiber alignment.

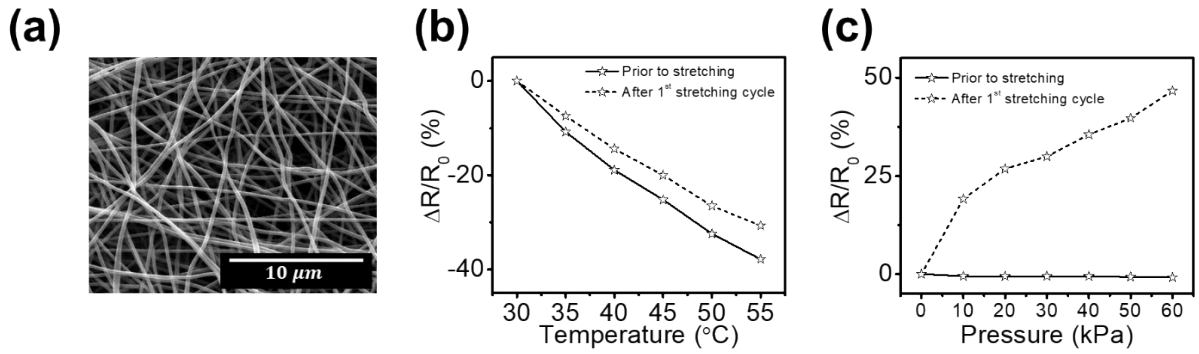

Figure S10. (a) SEM image of the RCNF film carbonized at 650 ℃ (RCNF-650). $\Delta R/R_0$ of the RCNF-650 sensor measured against (b) temperature and (c) pressure before and after uniaxial stretching.

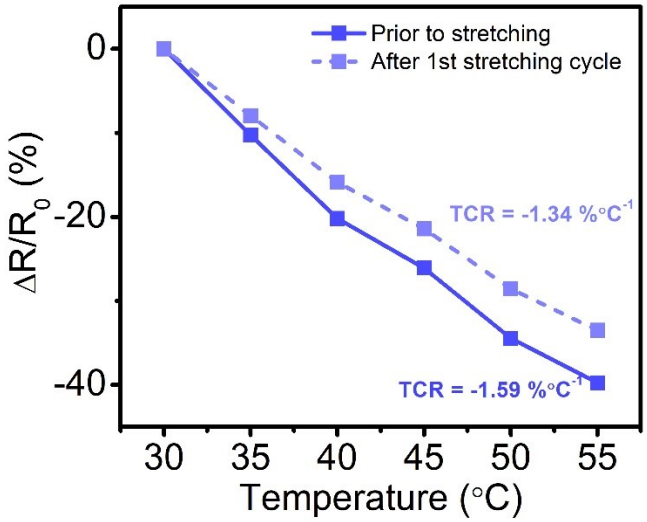

Figure S11. $\Delta R/R_0$ of the ACNF-650 sensor measured in the alignment direction against temperature before and after uniaxial stretching in the fiber alignment direction.

When the electrical resistances were measured in the fiber alignment direction, the ACNF-650 temperature sensor exhibited a TCR value of -1.59 %°C^{-1}, slightly better than that measured in the perpendicular direction (-1.52 %°C^{-1}). However, similar to the RCNF-650 sensor (Fig. S10), the temperature sensing performance of ACNF-650 significantly deteriorated after only one stretching cycle in the fiber alignment direction. When the fibers were subjected to a uniaxial tension, the CNF networks in the PDMS matrix were disrupted by fracture, but upon release of the applied tension the fractured CNFs were reconnected by physical contact to recover the conductive networks. Nevertheless, these physical contacts between the fractured CNFs were forced apart by the expanding PDMS during heating owing to their high thermal expansion coefficient of 3.2×10^{-4} °C^{-1}, increasing the electrical resistance and thus deteriorating the sensing performance. Therefore, the ACNF-650 films were placed with the fiber alignment perpendicular to the sensing direction so as to achieve the desired consistent sensing performance under uniaxial tension.

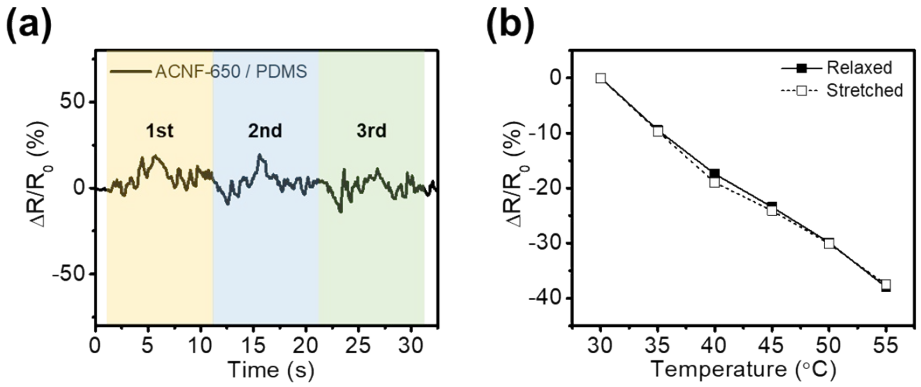

Figure S12. (a) $\Delta R/R_0$ of the ACNF-650 temperature sensor during 3 stretching cycles up to 50% strain. (b) Temperature-dependent $\Delta R/R_0$ of the ACNF-650 temperature sensor under relaxed and stretched conditions.

The ACNF temperature sensor presented small variations in electrical resistance during stretching cycles up to 50 % strain. The estimated gauge factor was less than 0.4, much smaller than the CNF strain sensor in our previous work.[23] This is because the temperature sensors were fabricated using ACNF films with fiber alignment perpendicular to the loading direction. In this case, the conductive networks of ACNFs remained mostly intact and interconnected when the sensor was stretched, exhibiting only small variations in electrical resistance (Fig. S9). In addtion, the ACNF sensor delivered consistent sensing performance even when stretched, with a response curve much the same as that measured without stretching, confirming its temperature sensing function regardless of mechanical loading (Fig. S12b).

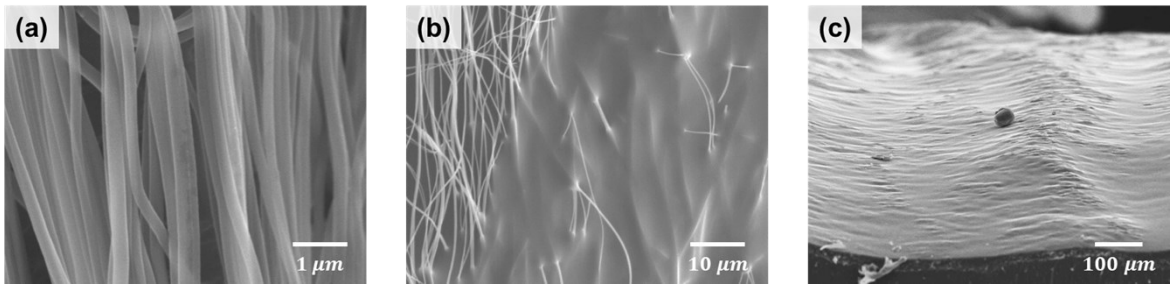

Figure S13. SEM images of (a) freestanding ACNFs showing physical contacts between individual fibers and (b) partially embedded ACNFs in a PDMS matrix. (c) Cross-sectional SEM image of the ACNF-650/PDMS composite produced via spin-coating.

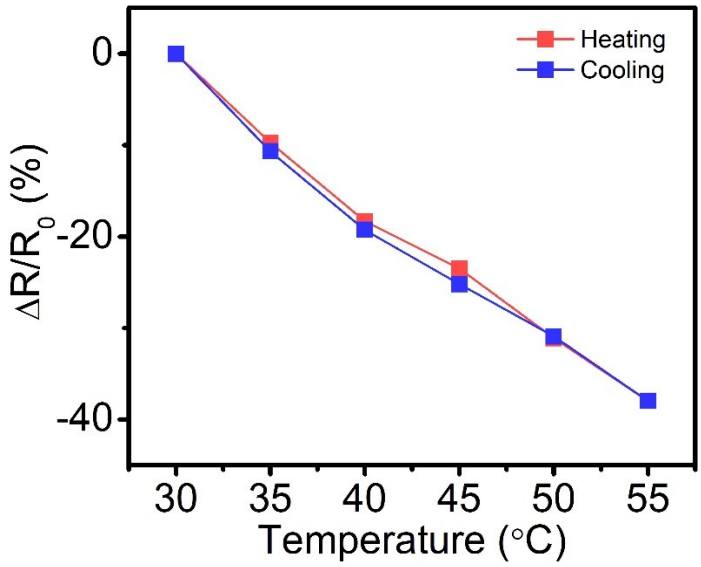

Figure S14. Hysteresis curve of the ACNF-650 temperature sensor.

The ACNF-650 temperature sensor suffered from a slight hysteresis because some heat was entrapped within the PDMS matrix during cooling. Consequently, the electrical resistances of the sensor during cooling were slightly lower than those recorded during heating.

Figure S15. Digital image of the data logger showing no reading, indicating that the electrical resistance was well over 100 MΩ for the ACNF-600/PDMS sensor.

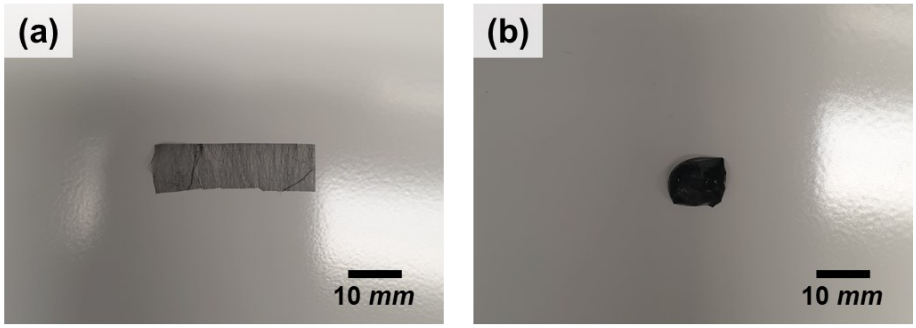

Figure S16. Freestanding ACNF film (a) before and (b) after dropping a water droplet on its surface.

Table S1. Thermal index (B) and activation energy (E_a) of the ACNF temperature sensors obtained from the Arrhenius model.

	B (*K*)	***E_a* (*meV*)**
ACNF-650	1855.29	319.75
ACNF-700	1255.79	216.43
ACNF-800	500.52	86.26
ACNF-900	151.03	26.03
ACNF-1000	46.93	8.09

B values are calculated from the slopes of the linear fits of $ln(R)$ *vs* T^{-1} curves (Fig. S5) and the corresponding E_a are obtained from the B values.

Table S2. Comparison of performance parameters between the current ACNF sensor and other carbon material-based flexible temperature sensors reported in the literature.

Temperature sensing materials	Sensitivity ($\%^{\circ}C^{-1}$)	Sensing range (°C)	Linearity	Insensitive stimuli*	Performance maintained after repeated stretching#	Reference
L-ascorbic acid rGO	1.30	25 ~ 45	Yes	(bending)	No	8
Solar rGO	0.74	25 ~ 150	No	/	No	39
IR rGO	1.48	15 ~ 165	No	/	No	40
Thermally rGO	1.05	30 ~ 100	No	/	Yes ($\varepsilon = 50\%$)	41
Hydrazine rGO	0.83	22 ~ 70	Yes	(pressure)	No	18
Vitamin C rGO	0.80	25 ~ 50	Yes	(strain)	Yes ($\varepsilon = 50\%$)	11
Hydrazine rGO	0.55	0 ~ 100	Yes	(strain/pressure/humidity)	Yes($\varepsilon = 3\%$)	42
Hydrazine and thermally rGO/PU	1.34	30 ~ 80	Yes	(strain)	Yes ($\varepsilon = 30\%$)	43
CVD grown graphene	0.42	25 ~ 50	Yes	/	Yes ($\varepsilon = 15\%$)	44
GNP	0.80	25 ~ 75	Yes	(strain)	Yes ($\varepsilon = 20\%$)	45
GWF	1.34	22 ~ 50	Yes	(humidity)	No	17
Graphene quantum dot	0.62	30 ~ 80	Yes	/	No	46
CNT + PEDOT:PSS	0.25	21 ~ 80	Yes	/	No	47
MWCNT	0.70	-48 ~ 150	Yes	/	No	20
Silk-based electrospun CNF	0.81	25 ~ 80	Yes	(pressure/ bending)	No	21
PAN-based electrospun ACNF	1.52	RT ~ 55	Yes	(pressure/ bending/ humidity)	Yes ($\varepsilon = 50\%$)	This work

* Temperature sensing performance unaffected by the stimuli mentioned in the brackets

Maximum strains applied in stretching cycles shown in the brackets